# Generative Phenomenology of form perception: Perceptograms and cortical models for amblyopic phantom percepts

Akihito Maruya[1],Bhavatharini Ramakrishnan[1], Farzaneh Olianezhad[1], Jingyun Wang[1], Jose-Manuel Alonso[1]& Qasim Zaidi[1*]

[1]*Graduate Center for Vision Research, State University of New York, New York, NY.*

[*]**Corresponding Author**

Qasim Zaidi
Graduate Center for Vision Research
State University of New York
33 West 42nd St
New York, NY 10036
USA

*Tel:* 862-202-2435
*Email:* qz@sunyopt.edu

Support: NEI grants EY035085 & EY035838

**ABSTRACT**

What we see is generated by our cortical neurons processing sensory input. Amblyopia provides a perfect case for studying the neural generation of percepts (Generative Phenomenology) because many amblyopes see phantom forms that contain more features than the stimulus through their amblyopic eye (AE) but not through the fellow eye (FE). Seeing phantom forms is unlike most visual disorders that lead to deficits and requires different types of models. Using computer guided dichoptic displays, we acquired perceptograms (viewable records of perceived images) for single gratings shown to AE. 92.6% of phantom percepts were matched exactly by plaid patterns made of two gratings shown to FE. A formal equation between the cortical signals generated by the gratings seen through AE with the signals generated by their perceptograms seen through FE was used to derive AE receptive fields as linear transforms of FE receptive fields. Passing gratings through the transformed AE model accurately generated the corresponding perceptograms. The transformations reflected complex changes in cortical receptive fields and output combinations. They also explained amblyopic deficits at discerning cyclic distortions from circularity and were validated via reverse-correlation. Changes in neuronal receptive fields thus have profound effects on perception, to the extent that observers can see more features than are present in what is viewed.

***Keywords***: visual perception | form perception | perceptual distortions | phantom percepts | receptive fields | visual disorders | amblyopia

## INTRODUCTION

If we could picture the percepts of people (or animals) and generate these images from cortical models (Generative Phenomenology), we could learn so much more than from experimental methods which only provide numerical estimates of parameters. Amblyopia, a disorder of spatial vision, provides an interesting case for a generative study of phenomenology because signals from the two eyes go through partially different cortical neuronal populations. Abnormal neural development in the cortex is a result of imbalance in the input from the two eyes caused by early misalignment of eyes (strabismus), unequal refractive power (anisometropia), or form deprivation (cataract)[1]. The disorder persists despite the restoration of good retinal image quality and eye health and affects 2-3% of the population. Consequently, many amblyopes see distorted versions of forms through the amblyopic eye (AE) but not through the fellow eye (FE). AE distortions can potentially be matched perfectly through the FE by rapidly generating images from a large set and using efficient search procedures. The matched images perform the function of a "Perceptogram", which is an externally viewable record of an internal perceptual image[2] or of perceptual distortions of a target image[3]. After obtaining the perceptogram, synthesizing it from generative cortical models can provide detailed insights into cortical processing and neural deficits, and teach us about how forms are created by the brain from the sensory input.

Striking form distortions seen by amblyopes had been noted for letters[4] and circular shapes[5], but the most diagnostic distortions were documented by showing high contrast sinusoidal gratings to the AE and drawing the percept through the FE[6,7]. The drawings of 20 out of 30 amblyopes fell into a few classes: correct grating orientation with an additional lower contrast grating at some oblique orientation, gratings with abrupt positional shifts orthogonal to the grating orientation, gratings with abrupt positional shifts oblique to the grating orientation, gaps in the grating, fragmented gratings, wavy appearance of straight gratings. The extra features drawn when viewing gratings are phantom percepts and the drawings were shown to resemble plaids formed by sums of

pairs of gratings[7], a key insight reproduced in Extended Figure E1. Forms are made of local orientations, which are initially extracted by neurons in primary visual cortex (V1) and then combined in later areas. Seeing phantom features is unlike most visual disorders in not being a deficit and requires new types of cortical models that transform the percept to add non-existent features instead of reducing it. The transformed processing likely starts with orientation encoding in V1[8] but also involves later mechanisms that decode orientation defined forms[9]. The systematic resemblance of the drawings to plaids ruled out neural scrambling[10,11] or systematic shifts in the neural map[12-14] as explanations. Phantom forms are potentially a bigger visual problem than the loss of 2 lines of visual resolution (the standard definition of amblyopia), so the complete lack of progress in this area in the last 20 years is surprising.

The accuracy of drawings depends on the observer's skill and the tools provided, and could misrepresent contrast, shading, spatial frequency (SF), orientation (OR), duty cycle, or linearity, so for higher fidelity, we measured perceptograms for 5 amblyopes ages 22-45 using computer generated stimuli. The resemblance of the drawn forms to sinusoidal plaids simplified stimulus generation. Observers viewed a dichoptic display, consisting of two orthogonally polarized LCDs passed through a beam splitter (Extended Figure E2) and seen through glasses polarized orthogonally so that one screen is seen exclusively by the AE and the other screen exclusively by the FE. The AE was shown a 3 dva (degrees of visual angle) test grating in the center (6, 9 or 12 cyc/deg, 0, 45, 90 or 135° orientations, ON or OFF). Either simultaneously or in alternating sequence, the FE was shown eight 3 dva patterns surrounding the test: 7 plaids matching the different phantom types illustrated in Figure E1, adjusted to the SF and OR of the test, plus an exact copy of the test grating (Figure 1A). The observer picked the pattern configuration most like the central image, ignoring possible differences in contrast, SF, OR and phase and scotomas. If the observer chose the identical grating, the trial ended. Otherwise, the display showed the AE just the test grating and adjacent to it showed the FE just the initially chosen match (Figure 1B). The chosen plaid was modified to generate better matches by varying contrast, SF, OR and phase of each of the 2 component gratings, until the percept of the test grating seen by the AE was matched perfectly by the generated

match in the FE. The procedure was repeated for each grating in three different sessions. Since the amblyopic phantoms have been well documented with a large sample[7], we concentrated on getting complete sets of perceptograms for the three amblyopes in our sample who saw phantoms and deriving a model of amblyopic cortex for each observer that could generate all the images including the veridical percepts.

The 24 matched ON and OFF perceptograms for each observer were used together to infer cortical neural deficits in the ON and OFF systems. We assumed the following linking hypothesis for our model: When the two patterns presented dichoptically look identical to an observer, the signals generated by the test grating seen through AE at some stage of visual cortex match the signals generated by the perceptogram seen through FE. As the simplest instance, we further assumed that AE V1 filters are linear transforms of FE V1 filters. For our model, we separately passed the image of the grating and the perceptogram through orientation-selective Steerable Filters representing a normal V1 cortex and then directly derived linearly transformed filters that collectively generated signals from single gratings that matched signals from perceptograms generated by the unmodified filters. The receptive fields (RF) of the modified filters showed changes in spatial frequency and orientation selectivity but also more complex changes, and a marked increase in spatial extent. The transformed filters can provide a target for physiological measurements, neural development models of amblyopic cortex and for tailoring treatments to ameliorate functional problems caused by amblyopia.

The processing deficits that led to the form phantoms could be adequately explained just in terms of linearly transformed RFs, so we next aimed to explain deficits in other form judgments that would require combinations or correlations of multiple filters. A diagnostic case is judging deviations from a perfectly circular blurred contour when it is replaced with a sinusoidal contour[15]. For a set of fixed frequencies of the distorting waveform, the threshold amplitude for the AE and FE to judge the presence of sinusoidal deviations provides a probe of global form processing[16]. We show that the AE filters derived for our observers, in conjunction with a rotational correlation, predict the change in thresholds for both eyes as a function of modulation frequency, with higher thresholds for the AE, consistent with the published data.

The form phantoms suggest deficits of orientation processing, but there is no direct method to test our models by measuring RFs of single neurons in human visual cortex. A recent reverse correlation study showed broader perceptive orientation tuning for the AE than for eyes of normal observers for vertical gratings[17], but our perceptograms show that some amblyopes see phantoms and some do not, and neither the phantoms nor the transformed filters are invariant to orientation. Consequently, for all our observers, we estimated perceptive fields[18] for 0, 45, 90 or 135° orientations of ON and OFF gratings separately for AE and FE using reverse correlation psychophysics[19-20]. Our observers found the task difficult, leading to noisy results especially for the AE, and the procedure cannot identify the cortical locus of the modified filters, but the perceptive orientation tuning through AE was broader, weaker, and shifted compared to FE orientation tuning for the observers who saw phantoms, but not for those who did not, providing additional insight into the orientation deficits underlying the form phantoms.

Note: A major component of this work is mathematical and computational. We explain the operations in words in the main text and present the mathematical details in the Supplemental Information under the same headings as the corresponding text sections.

## RESULTS

### Perceptograms

Three out of our 5 amblyopic observers (Table 1) reported seeing form phantoms in gratings shown to the AE, 60% versus 67% in the much larger sample[7]. Since each observer's images take up a lot of space, in the main text we present one observer's perceptograms and models in detail and present the others in the Supplementary Information. Figure 1C shows the 24 gratings and their corresponding perceptograms from a single session by Obs 3, who saw the largest number of phantoms. The left four columns display ON gratings, and the right four columns display OFF gratings: the same gratings are ON or OFF depending on being increments or decrements from a black or

white background respectively. Each orientation-frequency combination produced a distinct phantom pattern. Stimulus polarity also influenced perception: for example, at 90° and 6 cycles/deg, the ON grating produced a net-like appearance, while the OFF grating yielded a smoother, wavy structure with shadows at the top and bottom, suggesting that deficits could be different for the ON and OFF systems.

Complete sets of perceptograms from all three observers who saw phantoms are shown in Supplemental Figure S1, excluding the 12 cycles/deg condition for Obs 4, who reported only a uniform gray disk due to the spatial frequency exceeding their resolution limit. Across observers, the most frequently reported percepts resembled a grating with one or more blurred segments separating phase-shifts, like those illustrated in rows 2–5 of Figure E1. These patterns emerged from the combination of two gratings with closely matched spatial frequencies and contrast, but with slight differences in orientation and phase. The second most common patterns were net-like, resulting from the combination of one grating like the test and another with a lower spatial frequency, reduced contrast, and a different orientation (top row Figure E1). The bottom two patterns arise when the two constituent gratings are quite different in orientation from the test grating, with an interrupted pattern if they are the same contrast, and a wavy pattern if one is of lower contrast. The estimated perceptual distance between the perceptograms and the test gratings averaged over all the conditions for the three observers who saw phantoms was quantified as 0.204 and significantly different from 0.0 that denotes a perfect perceptual match by the Deep Image Structure and Texture Similarity (DISTS) metric[21]. The average perceptual distances between observers, spatial frequencies, orientations and ON/OFF polarities were not significantly different (Figure E4 Rows 1 & 2).

The summation of two sinusoidal gratings failed to fully capture the phantom percept only in 16 out of the 216 cases (7.4%). In these cases, observers verbally reported the mismatches—generally describing contrast mismatches. When contrast mismatches were insufficient descriptions, observers provided additional verbal descriptions (included in the far-right column of Figure S1), often reporting irregularities across the patterns. When verbal descriptions were inadequate, observers illustrated their percepts using Procreate on an iPad, after being trained to control linearity, width, contrast, shading and

orientation to make these drawings much more representative of the percept than the previously published pencil drawings. A few drawings showed some waviness not captured by the gratings. A careful drawing could take more than 30 minutes, making it unfeasible to use that method for the complete set of stimuli.

Across sessions, perceptograms were largely consistent within observers, with most variations reflecting minor differences in phase alignment. However, occasional session-to-session variability in reported pattern type was observed. For example, for ON gratings oriented at 0° with 6 cycles/deg frequency, Obs 3 reported a net-like pattern in two sessions but described a grating with a shadow in the third. The exact cause of this variability remains to be investigated, particularly fixation problems for the amblyopic eye.

The 92.6% of phantoms that were accepted as matched by the digitally generated plaids, along with the verbal descriptions and Procreate drawings of the rest, demonstrate the importance of measuring the perceptograms, because it seems that the lack of gradual shading in the published drawings leading to depictions as lines or square wave gratings, sometimes with unequal duty cycles, are due to limitations of drawing skills with pencil and paper and do not represent perceived phantoms. In addition, unlike the incomplete set of published drawings, we have complete sets of perceptograms for each observer, allowing us to build models that simultaneously account for both form phantoms and veridical percepts. Therefore, we build cortical models that reproduce perceptograms instead of the drawings. If the irregularities and waviness were frequent, we would have incorporated neural scrambling or under-sampling in the models, but the occurrences were too rare.

## Cortical model

We began with the working hypothesis that the form phantoms observed in amblyopia result from receptive field (RF) alterations in cells of early visual cortex that get input from the AE while the RFs are normal for cells that get input from the FE, with later visual areas processing the signals similarly irrespective of eye of origin. To model the responses of the

FE driven normal V1 cortex to the stimuli, we used steerable pyramids for frequency decomposition of input images in the Fourier domain[22]. This method is translation- and rotation-invariant, prevents aliasing, and allows for perfect reconstruction of the original image. The block diagram in Figure 2A (FE) illustrates the standard architecture of the complex steerable pyramid, and the supplemental section gives the mathematical details. The input image is first decomposed into high-pass and low-pass components by multiplying its Fourier transform with a high-pass filter that emphasizes higher spatial frequencies, and a low-pass filter that retains lower frequencies. Both filters are selective only for spatial frequency and are independent of orientation. The low-pass band is subsequently decomposed into oriented bandpass filters. The process in Figure 2A is repeated across the specified number of scales. To visualize the spatial profile of these filters, a centered delta function was passed through each filter and the inverse Fourier transform applied. The V1 filters for the FE are shown in Figure 2B for 16 orientations and four spatial scales arranged from high frequency (top) to low (bottom), each with 16 orientations. The resulting patterns resemble oriented Gabor filters and by passing perceptograms through the complete set of filters, we ascertained that they satisfy perfect reconstruction.

Our linking hypothesis is that the cortical representation of the test grating through AE neurons matches the cortical representation of the perceptogram through FE neurons. We tested if linear transforms applied to all standard oriented band-pass filters (Figure 2A AE) can collectively account for the cortical transformations, which allows us to write a formal equation equating the signals from the gratings through the linearly transformed filters to the signals from the perceptograms through the normal filters (SUPPLEMENTAL INFORMATION: Cortical model). The supplement shows that this equation can be simplified to directly derive the linear transformation from the ratio of the cross-spectrum to the power-spectrum. As an example, the transformed AE filters for Obs 3 for the ON and OFF conditions are visualized in Figure 2C. Comparing Figures 2B and 2C shows that some of the AE RF distortions could be changes in spatial frequency and orientation tuning of V1 cells, corresponding to linear operations of scaling and rotation, but others seem to create complex non-Gabor RFs suggesting combined operations including shearing,

particularly for diagonally oriented components. The transformed filters also exhibit an increase in effective spatial extent for the high frequencies as the ON and OFF lobes repeat over the complete 3 dva of the stimulus. The model cannot specify if these changes are in V1 RFs or in later combinations of V1 outputs. In particular, the greater spatial extent and some of the more complex changes could reflect broader spatial pooling of V1 outputs. Similar transformations are evident in the complete set of ON and OFF filters for Obs 3 & 4 who also saw phantom forms (Extended Figure E5).

We built models that covered all three spatial frequencies and four orientations, but separately for each observer, session, and stimulus type (ON vs. OFF). To test if each discrete set of linearly transformed filters is adequate, we applied the complete set in the Fourier domain (including the untransformed and unoriented high-pass and low-pass filters) to the Fourier transforms of the grating set, and then took the inverse Fourier transform to generate the corresponding perceptograms. An example comparison is shown in Figure 3 for the Obs 3 perceptograms from Figure 1C. Within each pair, the top image depicts the observer's perceptogram, while the bottom shows the corresponding reconstruction from the AE model. Comparisons for all perceptograms for all observers are presented in Supplemental Figure S1. Visual inspection shows that each model accurately predicts the observer's percepts with remarkable fidelity. The DISTS[21] estimated perceptual distance between the model generated and measured perceptograms averaged over all the conditions for the three observers who saw phantoms was 0.004 and not significantly different from 0.0 that denotes a perfect perceptual match. The average perceptual distances between observers, spatial frequencies, orientations and ON/OFF polarities were all not significantly different from 0.0 (Extended Figure E4 Rows 3 & 4).

**Sinusoidal Deformations from Circularity**

We tested our model on results of a task shown to have a global component: the detection of sinusoidal deviations from circularity of the fourth derivative of a Gaussian (D4)[16]. The left panel in Figure 4A shows the circular D4 stimulus and its log power spectrum, while

the right panel shows one of four sinusoidally deformed D4s, each with a radial frequency of 4, 6, 8 or 10 cycles per 360° with its corresponding log power spectrum. The circular D4 exhibits uniform power across all orientations, whereas the sinusoidally modulated D4s reveal localized increases in power at specific orientations, producing the same number of ridge-like structures in the spectrum as the number of cycles per 360°. As modulation amplitude increases, the local differences from the circular D4 (far left) become more perceptually apparent, and the ridges in the power spectrum more pronounced. Detecting these orientation-specific enhancements is critical for identifying deformation, but there is also a curvature detection aspect to this task beyond judging local orientation deviations. When the circular and modulated D4 stimuli were presented simultaneously, and the detection threshold for the modulation was measured separately for the AE and FE[15], detection thresholds for FE decreased with increasing radial frequency, but the AE thresholds were fairly constant and consistently higher than FE across all tested frequencies.

To investigate whether our AE V1 model can account for the observed difference in detection thresholds, we constructed a computational model with the schematic architecture shown in Figure 4B for the FE and AE simulations. In the fellow eye (FE) model, the circular D4 was processed through a simulated normal V1 pathway, and then we computed rotational correlations of the reconstructed image derived from the filter responses for rotation angles from −17° to 17° in 1° increments, yielding a feature vector of length 35. Feature vectors were computed similarly for modulated D4 stimuli with varying amplitudes and compared to the reference vector using a cosine similarity metric. In the amblyopic eye (AE) model, the same procedures were applied, but the stimuli were processed through the AE cortical model. This approach allowed us to quantitatively assess how closely the modulated stimuli resembled the circular reference under each cortical model.

The model predictions are presented in Figure 4C. Each panel represents a different radial frequency and compares the ON and OFF AE models to the FE models. Within each panel, cosine similarity is plotted as a function of modulation amplitude. Higher cosine similarity indicates greater representational overlap between the modulated and reference

stimuli, which predicts a higher detection threshold. In the FE cortex model, cosine similarity systematically decreases as the amplitude of modulation increases, and the rate of decrease is greater at higher radial frequencies, reflecting that cortical responses show increased sensitivity to higher-frequency deformations. These findings are consistent with the psychophysical results which demonstrated lower detection thresholds for higher-frequency deformations. In contrast, the AE cortex model exhibits relatively high cosine similarity between the modulated and reference D4 stimuli across all amplitudes and radial frequencies. This pattern is consistent with a diminished sensitivity to form deviations in the amblyopic cortex, consistent with the higher and constant thresholds reported for AE. This insensitivity is observed in both the ON and OFF models of the AE cortex, although the OFF model tends to produce slightly lower cosine similarity values than the ON model, indicating a modest difference in form perception between the two pathways.

**Orientation Tuning via Reverse Correlation**

The AE filters for amblyopes who see form phantoms show complex differences from the FE filters, but the perceptograms and D4 results clearly point to deficits in orientation processing. To understand differences in orientation tuning between amblyopes who see phantoms and amblyopes who do not, we measured perceptive fields using reverse correlation (RC)[18-20] for target gratings of 6 cyc/deg with 0°, 45°, 90°, or 135° orientation for ON and OFF conditions, separately for AE and FE (see Methods: Reverse Correlation). Participants fixated on the central display as a series of orientations were flashed and were instructed to press a button as soon as they detected the target orientation that had been shown to the FE. Given the difficulty that our amblyopic observers had doing the task, we used presentations of 100 msec, which is slower than usual. The supplemental section describes in detail how we obtained the orientation tuning curves shown in Figure 5. The left two columns (solid outlines; red for ON, blue for OFF) depict averaged responses from amblyopic participants who did not report form phantoms (No Phantoms Group). The

right two columns (dashed outlines) show data from participants who reported perceiving phantoms (Phantom Group). Each row corresponds to a different target orientation, and within each panel, response magnitude is plotted against the physical orientation of the stimulus. Red and blue dots represent the mean responses (based on 5,000 bootstrap resamples) for the amblyopic and fellow eyes, respectively. Solid curves denote the best fitting von Mises functions, with shaded bands indicating ±1 standard deviation. In the Non-Distortion Group, amblyopic and fellow eye tuning curves are roughly similar, but the Distortion Group clearly shows that the AE has reduced peak responses at 0° and 90°, broader tuning at 90°, and marked peak shifts at 45° and 135°. There are some differences between ON and OFF results as the ON curves are slightly broader, but they do not provide sufficient evidence that either system is more affected. Tuning curves for individual observers are plotted in Supplemental Figures E6 and E7.

## DISCUSSION

This paper solves a 20-year-old puzzle which has great significance for understanding amblyopic vision, and designing potential treatments, but the most significant conclusion comes from the generative part of the model showing that changes in neuronal receptive fields have profound effects on perception, to the extent that observers can see more features than are present in the viewed stimulus. The phantoms/distortions persist despite amblyopes having years to potentially adapt to the transformed RFs. The obvious inference is that receptive fields in normal visual cortex are exquisitely tuned for perception to be veridical in most cases.

The efficiency of orientation processing has been linked to the anisotropy in the distribution of image orientations in natural scenes being matched by the distribution of orientation tuned cells in V1[23]. The less-than-optimal consequence is that the anisotropy in the distribution of orientation and direction tuned cells, leads to anisotropy in the estimates of angles[9], orientation flows[9] and optic flows, which makes high level percepts of 3D shapes[9] and object non-rigidity[24] orientation-dependent, but leaves forms

recognizable. Distortions of receptive fields seem to be more disruptive of perception than variations in distributions of neuronal properties.

Amblyopia is clinically identified by a reduction in the visual acuity of the AE and disrupted binocular function, and these have been the focus of most research, and deficiencies in several low- and high-level perceptual abilities have also been documented. The phantoms, on the other hand, are hard to classify as a reduction. We definitively confirmed the published perceptual phantoms with perceptograms and showed that they can be explained by linear transformations of V1 RFs. Many transformed RFs resembled V1 RFs albeit with broader tuning and shifted peak, but others were much more complex and may reflect combinations of V1 outputs at later stages, compatible with orientation preference heterogeneity in Amblyopic V2[25,26].

Many of the linearly transformed filters in Figure 2C have many more lobes than the normal filters, which gives greater summation area for each RF and narrower tuning. This RF structure implies that the gratings that fill the whole RF while matching spatial frequency selectivity would evoke the maximum responses, unlike for normal RFs, which could partially explain the much larger increase in contrast sensitivity for amblyopes as compared to normals as field sizes are increased from 0.25 dva to 1.0 dva[27], although the greater increase up to field sizes of 8 dva would probably be due to enhanced lateral connections. The neural development of such abnormal RFs requires a larger spatial extent of inputs, whether it is thalamic inputs to V1 or V1 inputs to V2. Visual blur effectively reduces stimulus contrast, which would increase both the spatial footprint of lateral connectivity and its effect on visual responses[28]. During the amblyopic critical period, blur has been shown to reduce neuronal contrast sensitivity[29], but could also spread the formation of connections, leading to extended lateral connections, which could be tested physiologically along with the transformed RFs.

The formal equation between the AE response to gratings and the FE/V1 response to their matched perceptograms, enabled us to derive the transformed AE filters, but does not address their cortical loci. In principle the equation could be used to linearly transform a set of normal RFs in any cortical area, with the caveat that RFs are not too narrowly selective so that multiple RFs are responsive to multiple stimuli. If V2 RFs were as well

established as V1, we could have also applied the equation to V2, especially since amblyopia has been shown to disrupt RF structure in V2 neurons[25,26] possibly even more than it does in V1[27]. However, while it is known that V2 RFs are weighted combinations of large numbers of orientation tuned V1 RFs, and thus have much more intricate internal structure[30], which corresponds to heightened sensitivity to combinations of discontinuous orientations[31] and textures[32], there is no established canonical form that we could have used in the model.

The transformed AE RFs were not sufficient to explain the reduced sensitivity to the global judgement involving sinusoidal perturbations of contours, but required the addition of rotational correlation, which is more general than a model involving curvature specific neuronal connections[33]. Computational models of V2 neuronal sensitivities to naturalistic textures include many different correlations between V1 outputs[23,32], and it is likely that some V4 neurons that are sensitive to concentric stimuli[34] incorporate rotational correlations between earlier outputs.

The perceptual phantoms in the perceptograms consist of multiple oriented gratings which suggest broader tuning of orientation selectivity. Consistent with this idea, the results of the reverse correlation experiment showed orientation tuning differences between AE and FE for amblyopes who saw phantoms, but not for those that did not.

Amblyopia is generally thought to result from relative monocular deprivation of one eye causing a shift in ocular dominance of binocular neurons in V1 during an early critical period[35,36]. However, multiple instances of abnormalities in areas beyond V1[28,29] require more than a shift in ocular dominance[37]. Our results suggest that neural development of distortions in RFs need to be further investigated as a consequence of amblyopia. Our initial conjecture on starting this project was that the development of frequency and orientation selective V1 RFs requires balancing ON and OFF thalamic inputs[38], so if they are not balanced, RFs will not develop normally. We had also found some evidence that the ON system is affected more than the OFF in amblyopia, as measured by grating resolution and salience of whites versus blacks in random checkerboards[39], buttressing our idea. That provided the motivation to use separate ON and OFF gratings, but the perceptograms showed only a slightly stronger effect of

amblyopia for ON versus OFF stimuli, and the effects were mixed in the reverse correlation results. In the perceptogram measurements, the stimuli were seen for prolonged periods with eye movements and may not have isolated ON and OFF systems very well, but the reverse correlation stimuli were flashed briefly, so they truly are increments and decrements. In addition, a comparison of the AE filters to FE filters in Figure 2 reveals that whereas some RFs do become less selective in the AE, the transformation in other RFs is better described as rearrangements of segments and is not due solely to a weaker ON or OFF system. Our results thus do not provide strong support for our initial conjecture, and the neural development of abnormal RFs remains an open question, with broad effects of reduced contrast signals during the critical period being an important candidate.

It is worth considering the functional implications of our results. Stereo is compromised in amblyopia, so amblyopes have to rely on monocular cues. However, many monocular cues are critically based on orientation information, so if oriented patterns are perceived as distorted the brain may not be able to compensate. There is strong evidence for orientation information being critical for 3D shape from texture[40-42], mirror symmetry[43,44] and 3D pose perception[45]. Figure E8 shows that whereas the diagnostic orientation flows in a 3D shape from texture stimulus[41] are retained by the FE cortical model, they are lost by the AE model. Simulations using mirror symmetric complex images[43] showed loss of detail by the AE model and lack of symmetry in the output for some but not all images. Our models predict that the amblyopic eye will show greater deficiencies in these functions. It is possible that if the AE models were derived from a more diverse sample of perceptograms, the filters may extract more information from such images but investigating performance on these tasks for amblyopic observers that do and do not see form phantoms would be worthwhile, as it could also test whether the non-amblyopic eye is sufficient.

It took a combination of perceptual perceptogram measurements and generative computational modeling to reveal how neuronal RF properties lead to veridical and phantom percepts. Asymmetric matching has long been used as a psychophysical tool by putting the two eyes in different adaptation states, but the measured temporary differences

are small and not as dramatic as the stable differences between the perceptograms and the viewed stimuli, which are due to signals from the two eyes going through different cortical filters. Invasive methods for measuring fine-grained neuronal properties such as electrophysiology and 2-photon imaging cannot be done in humans, and it remains to be seen if recording and perceptography[3] in non-human primates can be expanded to a large enough scale. Non-invasive techniques such as fMRI and VEP would have to improve considerably in spatial and temporal resolution to answer such questions. We are exploring making more efficient and general Generative Phenomenology procedures by using generative adversarial networks[46] to search through human similarity space for plaid or broader classes of patterns[47] for the most probable perceptogram choice on each trial, with the observer's responses serving as part of the adversarial network. This will be particularly helpful in developmental studies of form perception with children. As a result, for the foreseeable future, Generative Phenomenology could be a powerful strategy to understand the neural bases of human perception.

## EQUIPMENT AND METHODS

### Observers

Five female observers with amblyopia participated in the study. The gender distribution was due to chance and not due to selective recruitment. Each had a prior clinical diagnosis of amblyopia and received a thorough optometric evaluation by the authors J.W. and B.R. prior to the experiment. Of the group, two had strabismic amblyopia and three had anisometropic amblyopia. Detailed participant data are presented in Table 1. All participants were unaware of the study's purpose and wore their best optical correction for the testing distance during the experiments. All participants provided written informed consent, and the study protocol was approved by the Institutional Review Board at the SUNY College of Optometry, in accordance with the tenets of the Declaration of Helsinki.

### Perceptograms

*Apparatus*

Figures 2A and 2B show the visual stimuli — test stimulus outlined in red and measuring stimuli outlined in blue — as presented using a Planar SD2620W Stereo/3D system. This setup consists of two calibrated LCD monitors positioned at right angles and optically combined using a beam splitter (see Figure E2). Each LCD monitor emits plane-polarized light, and the two monitor's polarization axes were mutually orthogonal. The image in the beam splitter is viewed through glasses polarized so each eye receives input from only one monitor: the amblyopic eye (AE) views the test stimulus, and the fellow eye (FE) views the measuring stimuli. Prior to the experiment, we confirmed the absence of crosstalk between the two eyes and ensured that all nine patterns appeared evenly spaced. For one participant (Obs 4) with strong interocular suppression, the test and motion stimuli were alternated at a rate set by the observer. Each eye received a display resolution of 1920 × 1200 pixels at a 60 Hz refresh rate. Stimuli were presented and the experiment was controlled using PsychoPy, and all data were analyzed using Python. Head position was stabilized with a chin rest at a viewing distance of 1.2 meters. All experiments were conducted in a darkened room.

*Stimulus generation*

Using Python, we generated 24 test gratings that varied in orientation (0°, 45°, 90°, and 135°), spatial frequency (6, 9, and 12 cycles/deg), and stimulus polarity (ON: black background producing bright bars; OFF: white background producing dark bars). Each stimulus subtended 3° of visual angle. Phantom patterns were created by summing pairs of gratings, as illustrated in Figure 1.

*Psychophysical procedures*

At the start of the experiment, we confirmed that all the participants could perceive a veridical grating through the fellow eye (FE) by asking them to verbally describe the single grating. In the main task, the amblyopic eye (AE) viewed a central single grating (red outline), while the FE was presented with a surrounding test grating and seven plaid patterns, each representing a different phantom type (blue outlines), as shown in Figure 1A. The observer selected the surrounding pattern that most closely matched the central grating. As illustrated in Figure 1B, they then fine-tuned four parameters each of the

component gratings of the selected plaid to improve the perceptual match. After adjustment, the observer judged whether the single grating viewed through the AE perceptually matched the plaid viewed through the FE. Gratings of the 4 orientations, 2 stimulus polarities, and 3 spatial frequencies, were presented in randomized order. Each session lasted approximately one hour, and the experiment was repeated on three separate days. If the perceptogram did not provide a perfect match, the observer first provided a verbal description of the mismatch. When verbal reports were insufficient, the observer sketched the perceived phantom using Procreate on a 12.9-inch iPad. The drawing was projected onto the Planar display seen by the FE, while the AE continued viewing the single grating.

**Reverse Correlation**

*Stimulus generation*

To measure orientation tuning, we presented a rapid sequence of sinusoidal gratings randomly varying in orientation at 10 Hz, with each grating displayed for 100 ms. This temporal frequency was chosen for task feasibility, as higher frequencies were too difficult for some participants with amblyopia. Gratings had a spatial frequency of 6.0 cycles/deg—the lowest frequency used in the Perceptogram experiment—and were shown at full contrast. Stimuli were presented on the front-facing monitor of the Planar Display, without the beam splitter, centrally through a 3° diameter circular aperture, against either a white or black background. Each condition consisted of one of four target orientations (0°, 45°, 90°, or 135°) combined with one of the two stimulus polarities (ON or OFF), and was tested separately for the fellow and amblyopic eyes, yielding a total of 16 unique conditions. Each trial within a condition consisted of 600 gratings presented over 60 seconds. Gratings were randomly selected from 10 possible orientations (spaced 18° apart) and one of four phases (0, $\pi/2$, $\pi$, or $3\pi/2$).

*Psychophysical procedures*

The experimental procedure followed protocols established in previous studies[17-20]. To assess each eye independently, participants wore an eye patch over the non-tested eye. Each trial consisted of a 1-minute sequence during which participants were instructed to

press a button as quickly as possible upon detecting a grating with a specific orientation (horizontal, vertical, or oblique) embedded within the sequence. Trials began with brief on-screen instructions, followed by a brief tone signaling the onset of the grating sequence. Participants initiated each trial with a button press and were instructed to maintain central fixation throughout. After each trial, the instruction screen reappeared, allowing participants to rest before continuing. No performance feedback was provided. Each condition included 30 trials, lasting approximately 45 minutes in total. The full set of conditions—four orientations, two stimulus polarities (ON and OFF), and two eyes (fellow and amblyopic)—was administered in randomized order, typically with two conditions completed per day.

**Data Availability**

All data and computational codes are available from the authors on request.

**Acknowledgments**

Supported by NEI grants EY035085 & EY035838.

**REFERENCES**

1. McKee, S. P., Levi, D. M., & Movshon, J. A. (2003). The pattern of visual deficits in amblyopia. *Journal of vision*, *3*(5), 5-5.
2. Tchertov, L. (2005). Perceptographic code in visual culture. *Sign Systems Studies*, *33*(1), 137-158.
3. Shahbazi, E., Ma, T., Pernuš, M., Scheirer, W., & Afraz, A. (2024). Perceptography unveils the causal contribution of inferior temporal cortex to visual perception. *Nature Communications*, *15*(1), 3347.
4. Pugh, M. (1958) Visual distortion in amblyopia Br J Ophthalmol 42,449-460
5. Sireteanu, R, Lagreze, WD, Constantinescu, DH. (1993) Distortions in two-dimensional visual space perception in strabismic observers Vision Res 33,677-690.

6. Hess, RF, Campbell, FW, Greenhalgh, T. (1978) On the nature of the neural abnormality in human amblyopia: neural aberrations and neural sensitivity loss Pflugers Arch 377,201-207.
7. Barrett, B. T., Pacey, I. E., Bradley, A., Thibos, L. N., & Morrill, P. (2003). Nonveridical visual perception in human amblyopia. *Investigative Ophthalmology & Visual Science*, *44*(4), 1555-1567.
8. Sharma, V, Levi, DM, Coletta, NJ. (1999) Sparse sampling of gratings in the visual cortex of strabismic amblyopes Vision Res 39,3526-3536
9. Cohen, E. H., & Zaidi, Q. (2007). Fundamental failures of shape constancy resulting from cortical anisotropy. Journal of Neuroscience, 27(46), 12540-12545.
10. Hess, R. F. (1982). Developmental sensory impairment: amblyopia or tarachopia? Human neurobiology, 1(1), 17-29.
11. Hess, RF, Field, DJ, Watt, RJ. (1990) The puzzle of amblyopia. Blakemore, C eds. Vision Coding and Efficiency ,267-280 Cambridge University Press Cambridge, UK.
12. Sireteanu, R., & Fronius, M. (1989). Different patterns of retinal correspondence in the central and peripheral visual field of strabismics. Investigative ophthalmology & visual science, 30(9), 2023-2033.
13. Hess, R. F., & Field, D. J. (1994). Is the spatial deficit in strabismic amblyopia due to loss of cells or an uncalibrated disarray of cells?. Vision research, 34(24), 3397-3406.
14. Lagreze, W. D., & Sireteanu, R. (1991). Two-dimensional spatial distortions in human strabismic amblyopia. Vision research, 31(7-8), 1271-1288.
15. Hess, R. F., Wang, Y. Z., Demanins, R., Wilkinson, F., & Wilson, H. R. (1999). A deficit in strabismic amblyopia for global shape detection. Vision research, 39(5), 901-914.
16. Wilkinson, F., Wilson, H. R., & Habak, C. (1998). Detection and recognition of radial frequency patterns. Vision research, 38(22), 3555-3568.
17. Zhu, J., Ruan, X., Li, C., Yuan, J., Yang, Y., Zhang, W., ... & Hou, F. (2022). Psychophysical Reverse Correlation Revealed Broader Orientation Tuning and

Prolonged Reaction Time in Amblyopia. Investigative Ophthalmology & Visual Science, 63(5), 3-3.

18. Neri, P., & Levi, D. M. (2006). Receptive versus perceptive fields from the reverse-correlation viewpoint. Vision research, 46(16), 2465-2474.
19. Ringach, D. L., Sapiro, G., & Shapley, R. (1997). A subspace reverse-correlation technique for the study of visual neurons. Vision research, 37(17), 2455-2464.
20. Ringach, D. L. (1998). Tuning of orientation detectors in human vision. Vision research, 38(7), 963-972.
21. Ding, K., Ma, K., Wang, S., & Simoncelli, E. P. (2020). Image quality assessment: Unifying structure and texture similarity. *IEEE transactions on pattern analysis and machine intelligence*, *44*(5), 2567-2581.
22. Simoncelli, E. P., & Freeman, W. T. (1995). The steerable pyramid: A flexible architecture for multi-scale derivative computation. In Proceedings., international conference on image processing (Vol. 3, pp. 444-447). IEEE.
23. Girshick, A. R., Landy, M. S., & Simoncelli, E. P. (2011). Cardinal rules: visual orientation perception reflects knowledge of environmental statistics. Nature neuroscience, 14(7), 926-932.
24. Maruya, A., & Zaidi, Q. (2025). Anisotropy of object nonrigidity: High-level perceptual consequences of cortical anisotropy. *bioRxiv*, doi: https://doi.org/10.1101/2024.09.10.612333
25. Bi, H., Zhang, B., Tao, X., Harwerth, R. S., Smith III, E. L., & Chino, Y. M. (2011). Neuronal responses in visual area V2 (V2) of macaque monkeys with strabismic amblyopia. *Cerebral cortex*, *21*(9), 2033-2045.
26. Tao, X., Zhang, B., Shen, G., Wensveen, J., Smith, E. L., Nishimoto, S., ... & Chino, Y. M. (2014). Early monocular defocus disrupts the normal development of receptive-field structure in V2 neurons of macaque monkeys. *Journal of Neuroscience*, *34*(41), 13840-13854.
27. Hagemans, K. H., & Van Der Wildt, G. J. (1979). The influence of the stimulus width on the contrast sensitivity function in amblyopia. *Investigative Ophthalmology & Visual Science*, *18*(8), 842-847.

28. Nauhaus, I., Busse, L., Carandini, M., & Ringach, D. L. (2009). Stimulus contrast modulates functional connectivity in visual cortex. *Nature neuroscience*, *12*(1), 70-76.
29. Movshon, J. A., Eggers, H. M., Gizzi, M. S., Hendrickson, A. E., Kiorpes, L., & Boothe, R. G. (1987). Effects of early unilateral blur on the macaque's visual system. III. Physiological observations. *Journal of Neuroscience*, *7*(5), 1340-1351.
30. Hassanpour, M. S., Merlin, S., Federer, F., Zaidi, Q., & Angelucci, A. (2024). Primate V2 Receptive Fields Derived from Anatomically Identified Large-Scale V1 Inputs. bioRxiv 2024.03.22.586002; doi: https://doi.org/10.1101/2024.03.22.586002.
31. Schmid, A. M., Purpura, K. P., Ohiorhenuan, I. E., Mechler, F., & Victor, J. D. (2009). Subpopulations of neurons in visual area v2 perform differentiation and integration operations in space and time. *Frontiers in systems neuroscience*, *3*, 915.
32. Freeman, J., Ziemba, C. M., Heeger, D. J., Simoncelli, E. P., & Movshon, J. A. (2013). A functional and perceptual signature of the second visual area in primates. Nature neuroscience, 16(7), 974-981
33. Poirier, F. J., & Wilson, H. R. (2006). A biologically plausible model of human radial frequency perception. *Vision research*, *46*(15), 2443-2455.
34. Gallant, J. L., Braun, J., & Van Essen, D. C. (1993). Selectivity for polar, hyperbolic, and Cartesian gratings in macaque visual cortex. Science, 259(5091), 100-103.
35. Hubel, D. H., Wiesel, T. N., & LeVay, S. (1976, January). Functional architecture of area 17 in normal and monocularly deprived macaque monkeys. In *Cold Spring Harbor Symposia on Quantitative Biology* (Vol. 40, pp. 581-589). Cold Spring Harbor Laboratory Press.
36. Hensch, T. K., & Quinlan, E. M. (2018). Critical periods in amblyopia. Visual neuroscience, 35, E014.
37. Kiorpes, L. (2019). Understanding the development of amblyopia using macaque monkey models. Proceedings of the National Academy of Sciences, 116(52), 26217-26223.

38. Najafian, S., Koch, E., Teh, K. L., Jin, J., Rahimi-Nasrabadi, H., Zaidi, Q., ... & Alonso, J. M. (2022). A theory of cortical map formation in the visual brain. Nature communications, 13(1), 2303.
39. Pons, C., Jin, J., Mazade, R., Dul, M., Zaidi, Q., & Alonso, J. M. (2019). Amblyopia affects the ON visual pathway more than the OFF. Journal of Neuroscience, 39(32), 6276-6290.
40. Li, A., & Zaidi, Q. (2000). Perception of three-dimensional shape from texture is based on patterns of oriented energy. Vision research, 40(2), 217-242.
41. Li, A., & Zaidi, Q. (2004). Three-dimensional shape from non-homogeneous textures: carved and stretched surfaces. Journal of Vision, 4(10), 3-3.
42. Fleming, R. W., Holtmann-Rice, D., & Bülthoff, H. H. (2011). Estimation of 3D shape from image orientations. *Proceedings of the National Academy of Sciences*, *108*(51), 20438-20443.
43. Rainville, S. J., & Kingdom, F. A. (2000). The functional role of oriented spatial filters in the perception of mirror symmetry—psychophysics and modeling. *Vision Research*, *40*(19), 2621-2644.
44. Cohen, E. H., & Zaidi, Q. (2013). Symmetry in context: Salience of mirror symmetry in natural patterns. Journal of Vision, 13(6), 22-22.
45. Koch, E., Baig, F., & Zaidi, Q. (2018). Picture perception reveals mental geometry of 3D scene inferences. Proceedings of the National Academy of Sciences, 115(30), 7807-7812.
46. Denton, E. L., Chintala, S., & Fergus, R. (2015). Deep generative image models using a laplacian pyramid of adversarial networks. *Advances in neural information processing systems*, *28*.
47. Gatys, L., Ecker, A. S., & Bethge, M. (2015). Texture synthesis using convolutional neural networks. *Advances in neural information processing systems*, *28*.

| Subject | Age | Gender | Type of amblyopia | Visual Acuity(LogMAR) | Refraction | Fixation | Distortion |
|---|---|---|---|---|---|---|---|
| Obs 1 | 24 | F | Anisometropic | OD: 0.00<br>OS: 0.20 | OD: +6.75/-0.25 X 125<br>OS:+7.75/-1.00 X 075 | Central | No |
| Obs 2 | 49 | F | Combined | OD:0.20<br>OS:0.00 | OD: +5.50<br>OS: +5.00 | Central | No |
| Obs 3 | 22 | F | Anisometropic | OD:0.00<br>OS: 0.30 | OD: -2.50/-1.00 X 180<br>OS: +0.75/-1.00 X 180 | Central | Yes |
| Obs 4 | 22 | F | Combined | OD: 1.00<br>OS:0.00 | OD: -22.00/-2.00 X 035<br>OS: -11.50/-2.75 X 140 | Temporal | Yes |
| Obs 5 | 23 | F | Anisometropic | OD: 0.40<br>OS: -0.10 | OD: 0.00/-0.50 X 018<br>OS: -3.25/-0.50 X 121 | Central | Yes |

**Table 1.** Observer details.

A

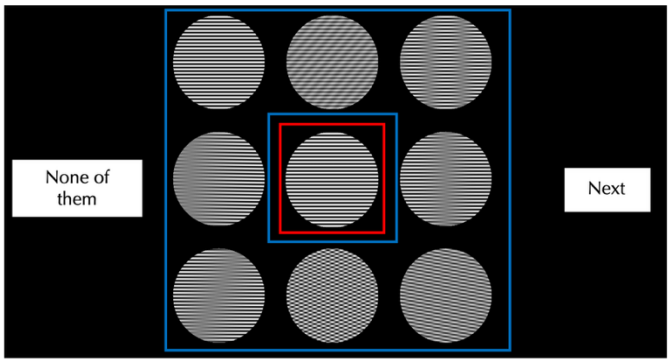


B

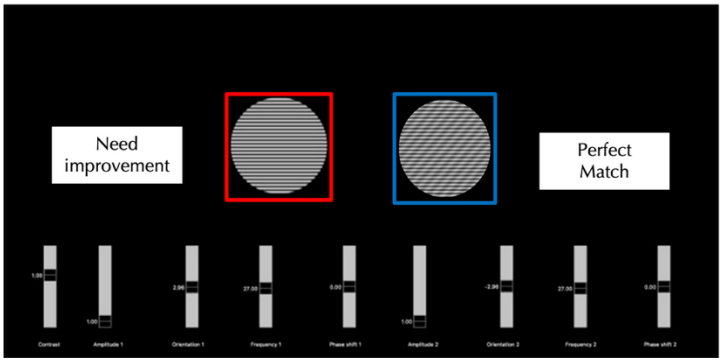


C

# Perceptograms

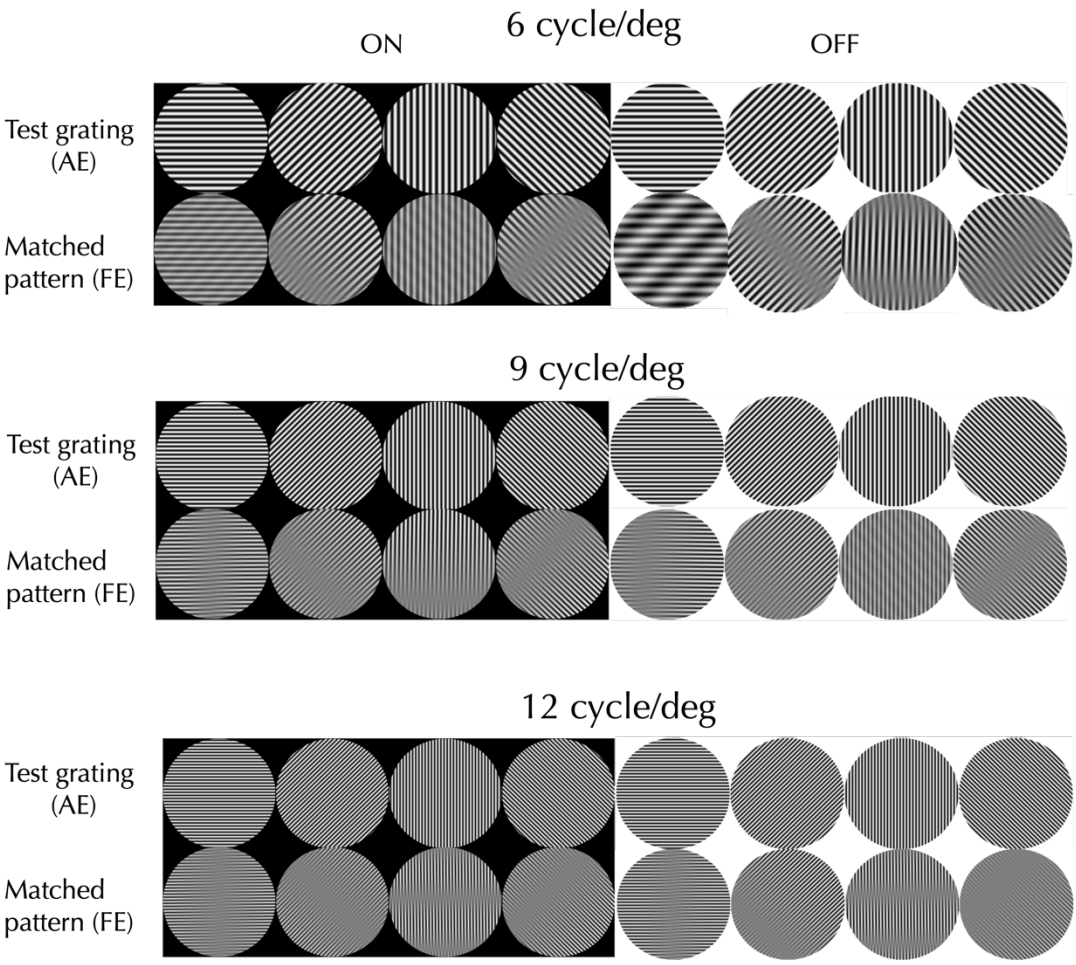

**Figure 1. Perceptogram Procedure and Images:**

**A. Initial Configuration:** The amblyopic eye (AE) views a central single grating (red border), while the fellow eye (FE) sees a surrounding test grating and seven plaid patterns, each representing a different distortion type (blue borders). The observer selects the surrounding pattern that most closely matches the central grating.

**B. Matching Procedure:** The observer fine-tunes four parameters of each of the two gratings within the selected plaid pattern seen by the FE to make a perceptual match to what the AE sees when shown the test grating.

**C. Results:** Eight ON and OFF gratings per spatial frequency and the corresponding perceptograms are shown for Obs 3 for one session.

A

FE

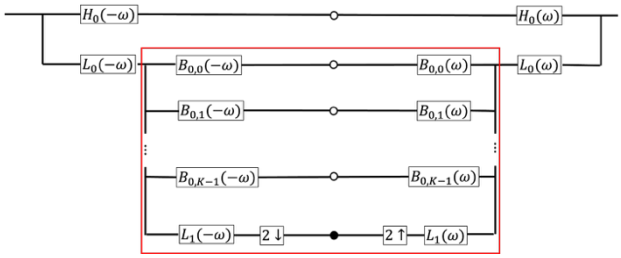


AE

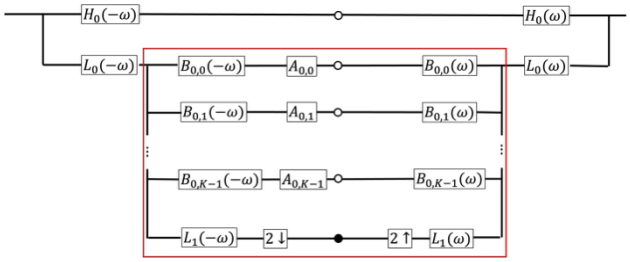


B

FE Cortex

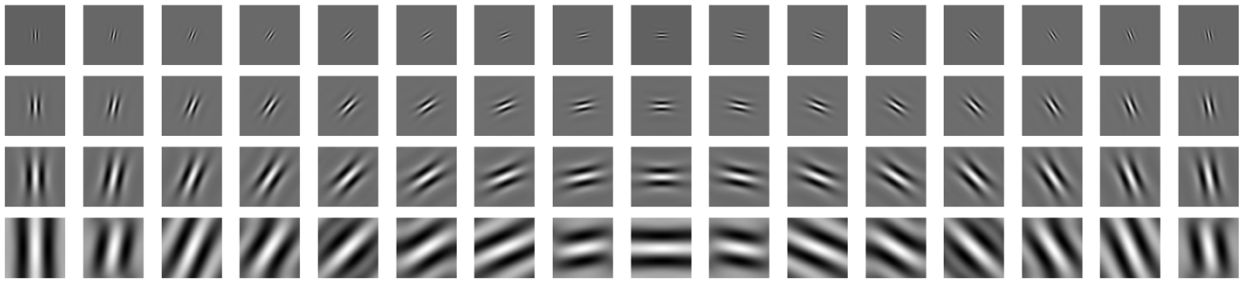

C

AE Cortex

ON

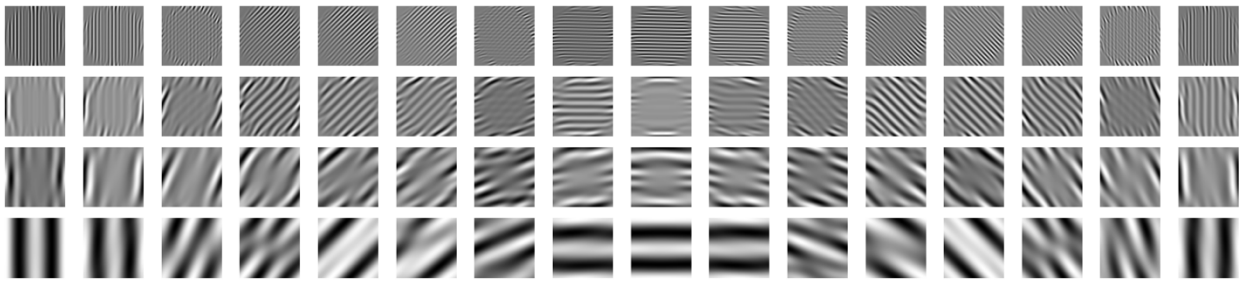

OFF

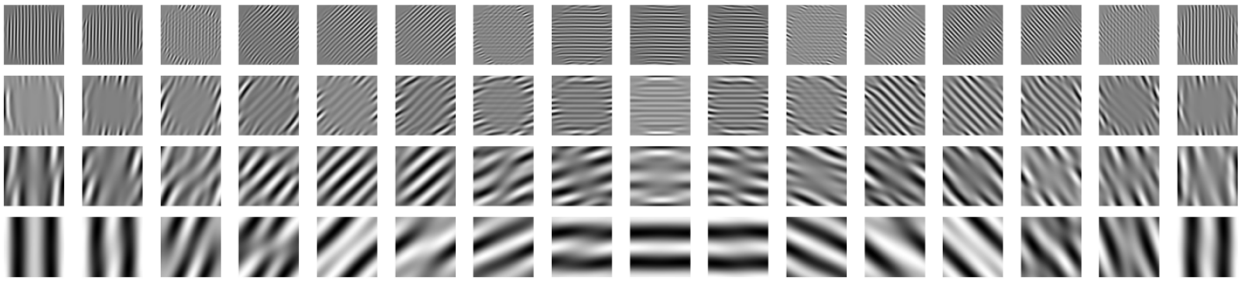

**Figure 2. Cortical Model.**

**A (FE). Standard Steerable Pyramid:** The left side shows the complex steerable pyramid decomposition, and the right side shows the reconstruction process. The input image is split into high- and low-pass bands. The low-pass band is further decomposed into a lower-frequency band and a set of orientation sub-bands. White dots represent single sub-bands, while black dots denote sub-bands at the next coarser scale. The symbols ↓ and ↑ indicate downsampling and upsampling operations, respectively. The region outlined in red is repeated across a specified number of scales.
**A (AE) Modified Pyramid:** A linear Amblyopic Transformation $A_{i,k}$ is applied to each band-pass oriented filter.
**B: Fellow Eye Filters:** Visualization of each orientation sub-band from the standard steerable pyramid, representing the FE cortex, showing the response to a central impulse.
**C: Amblyopic Eye Filters:** Visualization of each orientation sub-band from the linearly transformed amblyopic steerable pyramid in response to a central impulse, representing the AE ON and OFF cortical RFs for Obs 3.

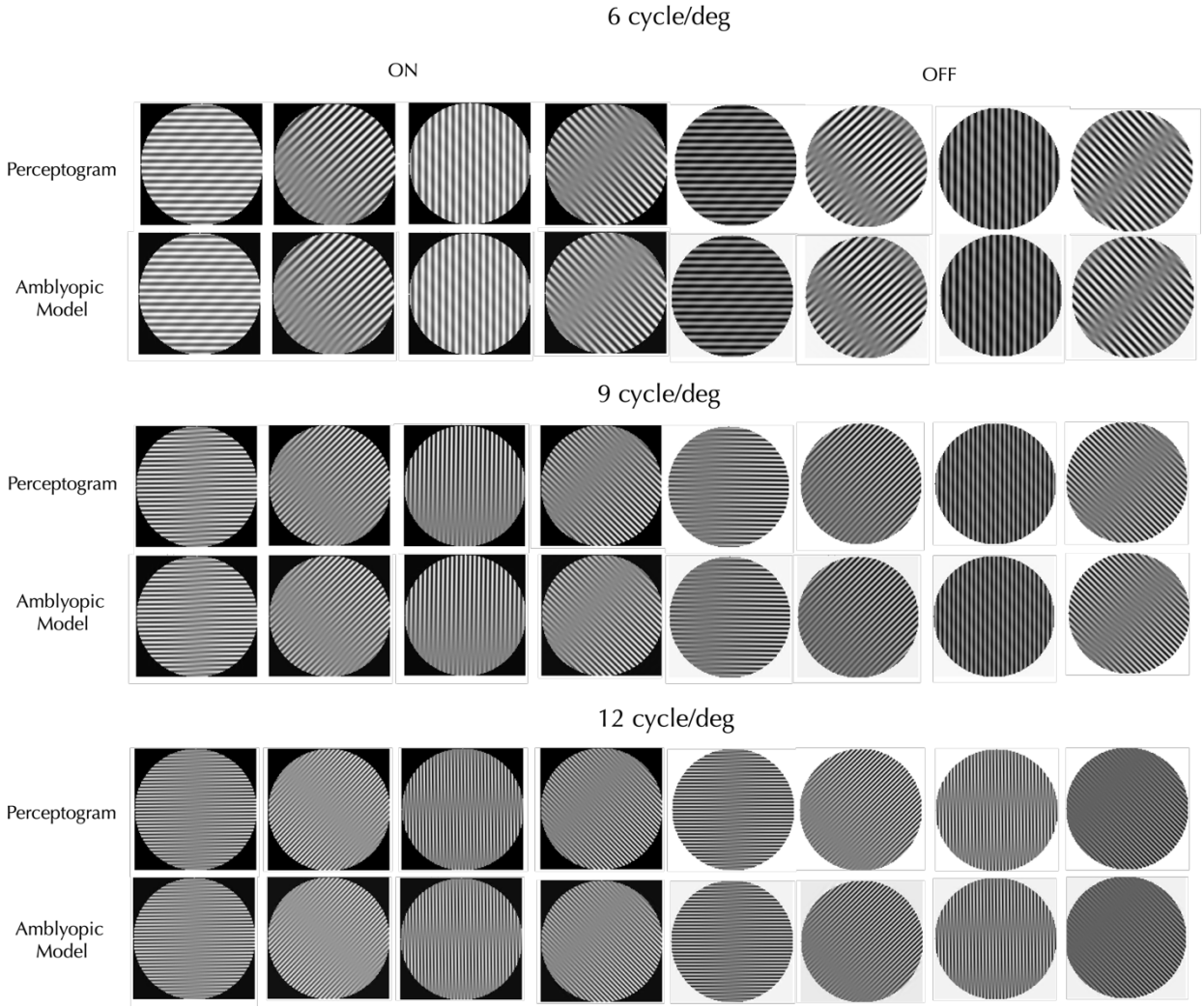


**Figure 3. Perceptograms vs. Model Reconstructions.**

The left four panels correspond to ON stimuli, while the right four correspond to OFF stimuli. Each column represents a different stimulus orientation (the same stimulus sequence as Figure 1C). Within each stimulus pair, the top image shows the observer's perceptogram, and the bottom image shows the corresponding reconstruction from the linearly transformed V1 filters representing the AE cortex. The model accurately generates the perceptograms.

A

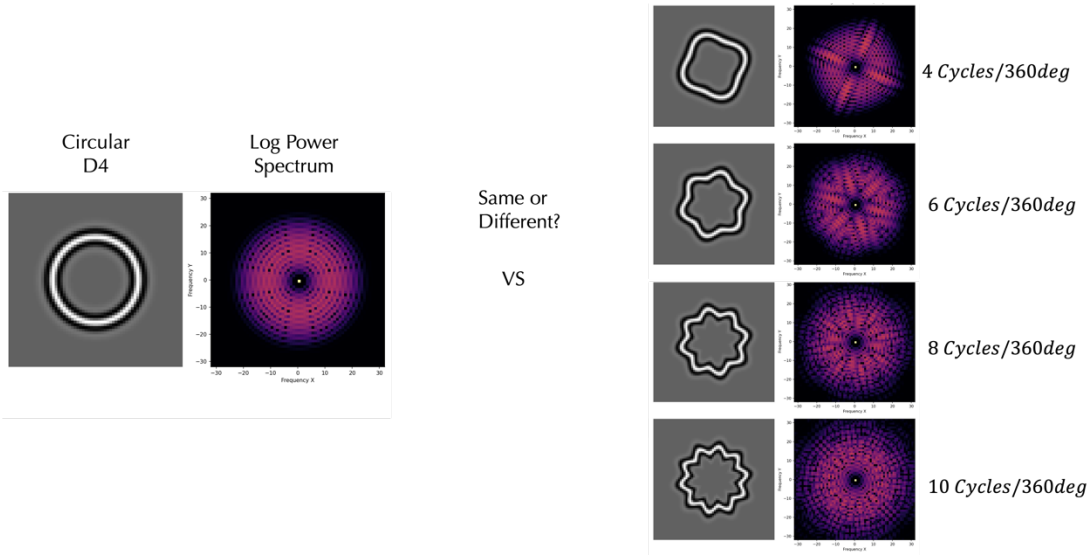
Circular
D4
Log Power
Spectrum
Same or
Different?
VS
4 Cycles/360deg
6 Cycles/360deg
8 Cycles/360deg
10 Cycles/360deg

B

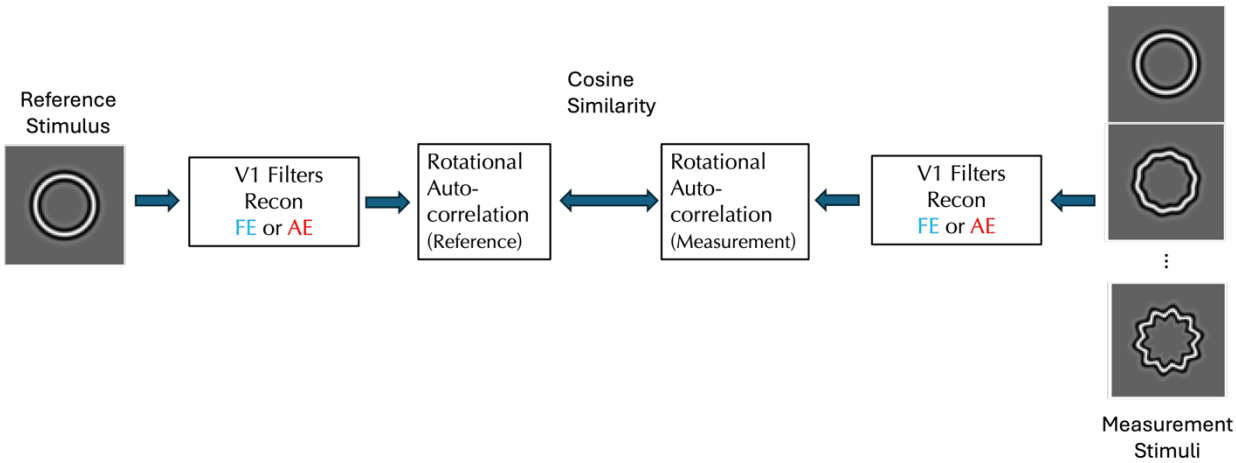
Reference
Stimulus
V1 Filters
Recon
FE or AE
Rotational
Auto-
correlation
(Reference)
Cosine
Similarity
Rotational
Auto-
correlation
(Measurement)
V1 Filters
Recon
FE or AE
Measurement
Stimuli

C

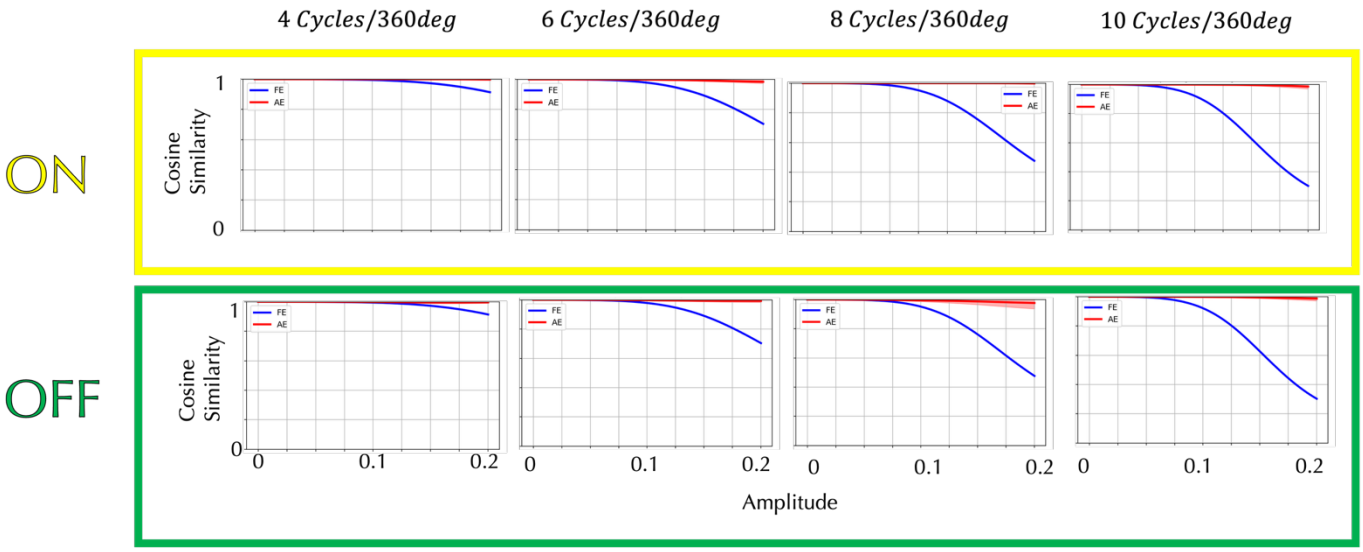
4 Cycles/360deg
6 Cycles/360deg
8 Cycles/360deg
10 Cycles/360deg
ON
OFF
Cosine
Similarity
1
0
FE
AE
0
0.1
0.2
Amplitude

**Figure 4. Detection of Sinusoidal Deformations from Circular D4 Stimuli and Model Simulations.**

**A:** Circular and deformed D4 stimuli and their log power spectra. While the circular D4 displays uniform power across orientations, the deformed D4s show localized increases in power at specific orientations, forming ridge-like structures. Amblyopic eyes consistently exhibited higher amplitude thresholds across radial frequencies than fellow eyes.

**B:** Model for responses of the fellow eye and amblyopic eye. The statistical representation of the circular D4, processed through either the fellow eye (FE) or amblyopic eye (AE) V1 filters and then through a rotational correlation, is compared to those of the modulated D4 stimuli at various amplitudes using cosine similarity.

**C:** The top row shows predictions from the ON amblyopic model (Yellow box), and the bottom row from the OFF amblyopic model (Green box), averaged over the observers who saw distortions (shading indicating ±1 standard deviation). Each row corresponds to a different radial frequency (4–10 cycles/360°). Each panel plots cosine similarity as a function of amplitude, where a higher similarity leads to a higher detection threshold. For the FE (black curves), cosine similarity decreases with increasing amplitude, and this reduction is more pronounced at higher radial frequencies. The AE curves (red) show relatively high cosine similarity across amplitudes and radial frequencies. Both are consistent with published results.

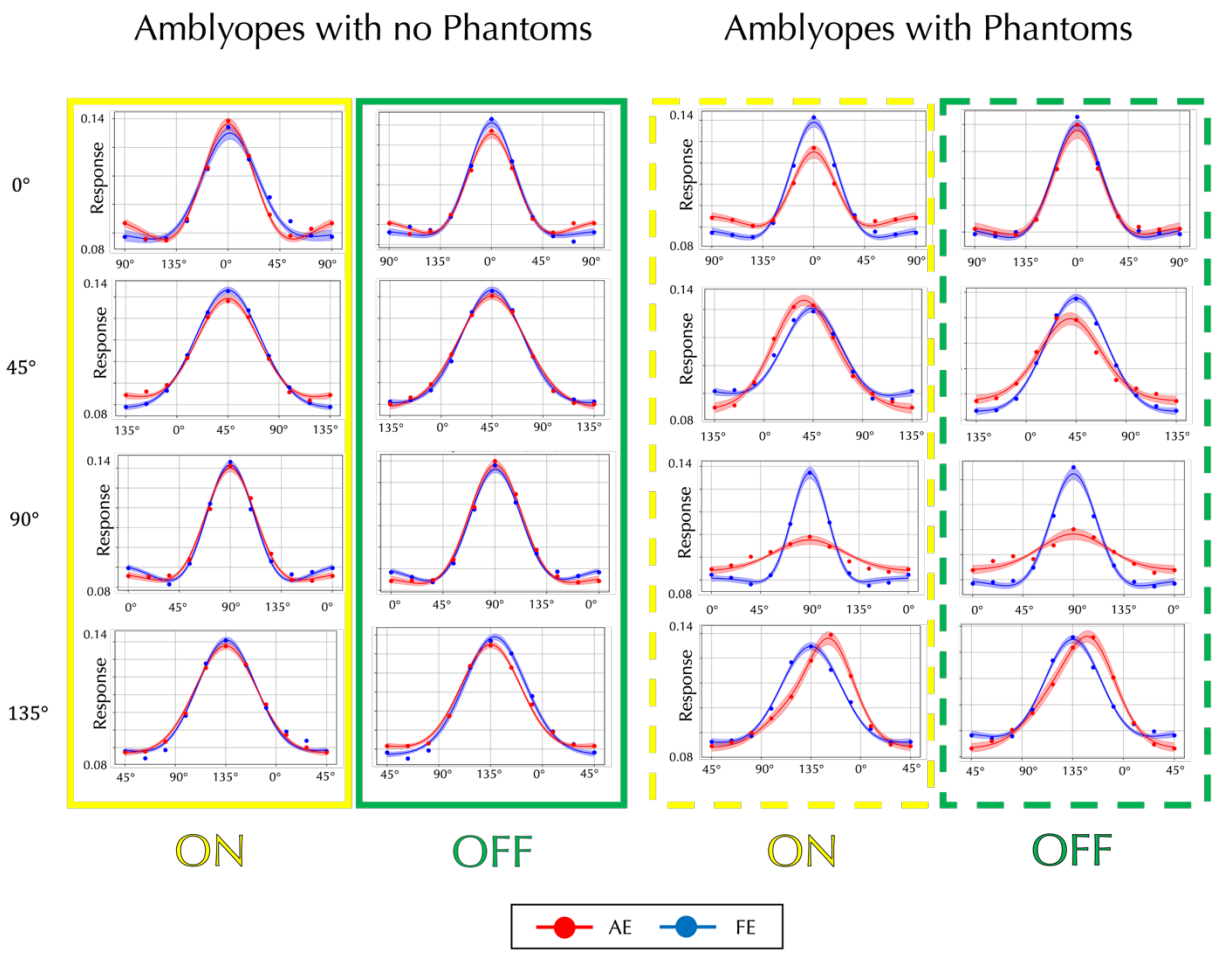


**Figure 5. Perceptual Orientation Tuning Curves for Non-Distortion vs. Distortion Groups.** The left two columns show the average results for amblyopic participants who did **not** report form distortions (Solid boxes Yellow: ON, Green: OFF). The right two columns (Dashed boxes) show results for those who **did** report distortions. Each row corresponds to a different target orientation. Within each panel, response magnitude is plotted against physical orientation. Response magnitude is scaled to give unit area under the curve. Red and blue dots represent the mean responses (after 5,000 bootstrap resamples) for the amblyopic and fellow eye conditions, respectively. Solid traces are the best fitting von Mises functions, with shaded areas indicating ±1 standard deviation. Most of the mean R-squared values were 0.98 or higher.

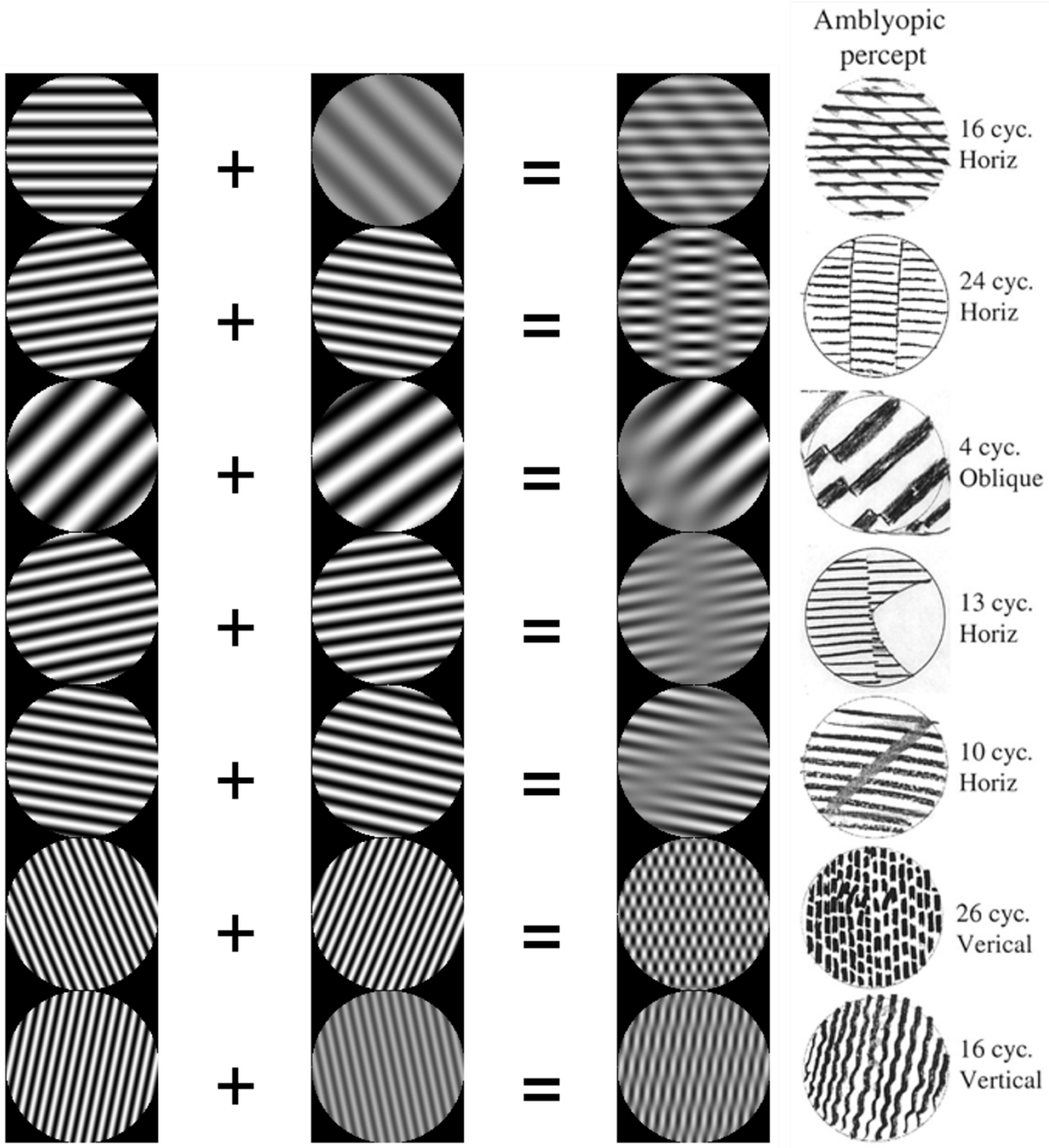


**Figure E1. Drawings made by amblyopes matched by plaids consisting of sums of gratings:**
Right: Drawings of seven classes of phantom percepts evoked by the sinusoidal gratings described by # cycles and orientation. Middle: Plaids resembling the drawn phantoms, produced by sums of two component gratings. Left: Component gratings.

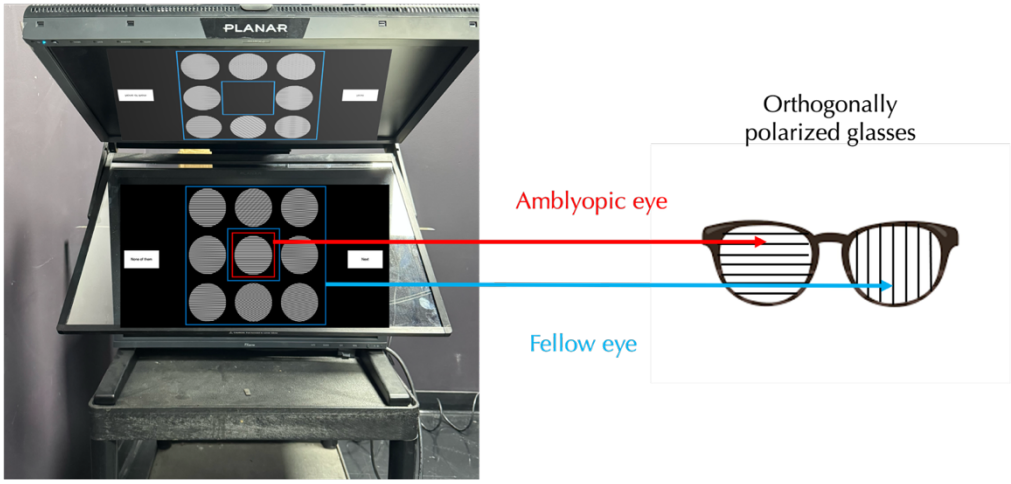


**Figure E2. Dichoptic display using two monitors and a beam splitter (Planar Inc SD2620W):** Images from two LCD monitors with orthogonal polarization are viewed through a beam splitter that aligns the two images for an observer. The observer wears glasses with the left eyepiece polarized to block one of the images and the right eyepiece polarized orthogonally to block the other. During the experiment, the central single grating was shown to the amblyopic eye, while the surrounding stimuli were presented to the fellow eye.

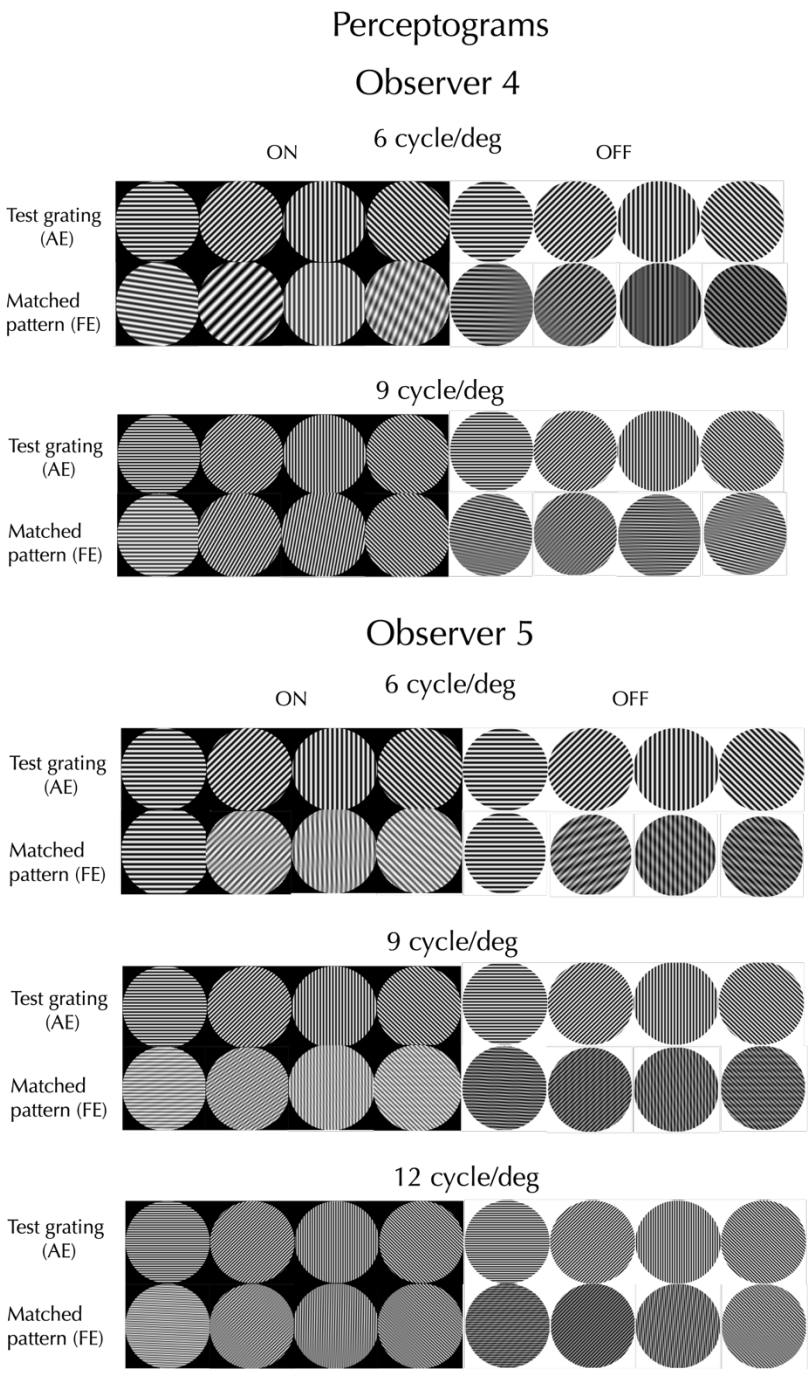


**Figure E3. Perceptograms:** Eight ON and OFF gratings per spatial frequency and the corresponding perceptograms are shown for Obs 4 & 5 for one session. Obs 4 could not resolve 12 cycle/deg gratings.

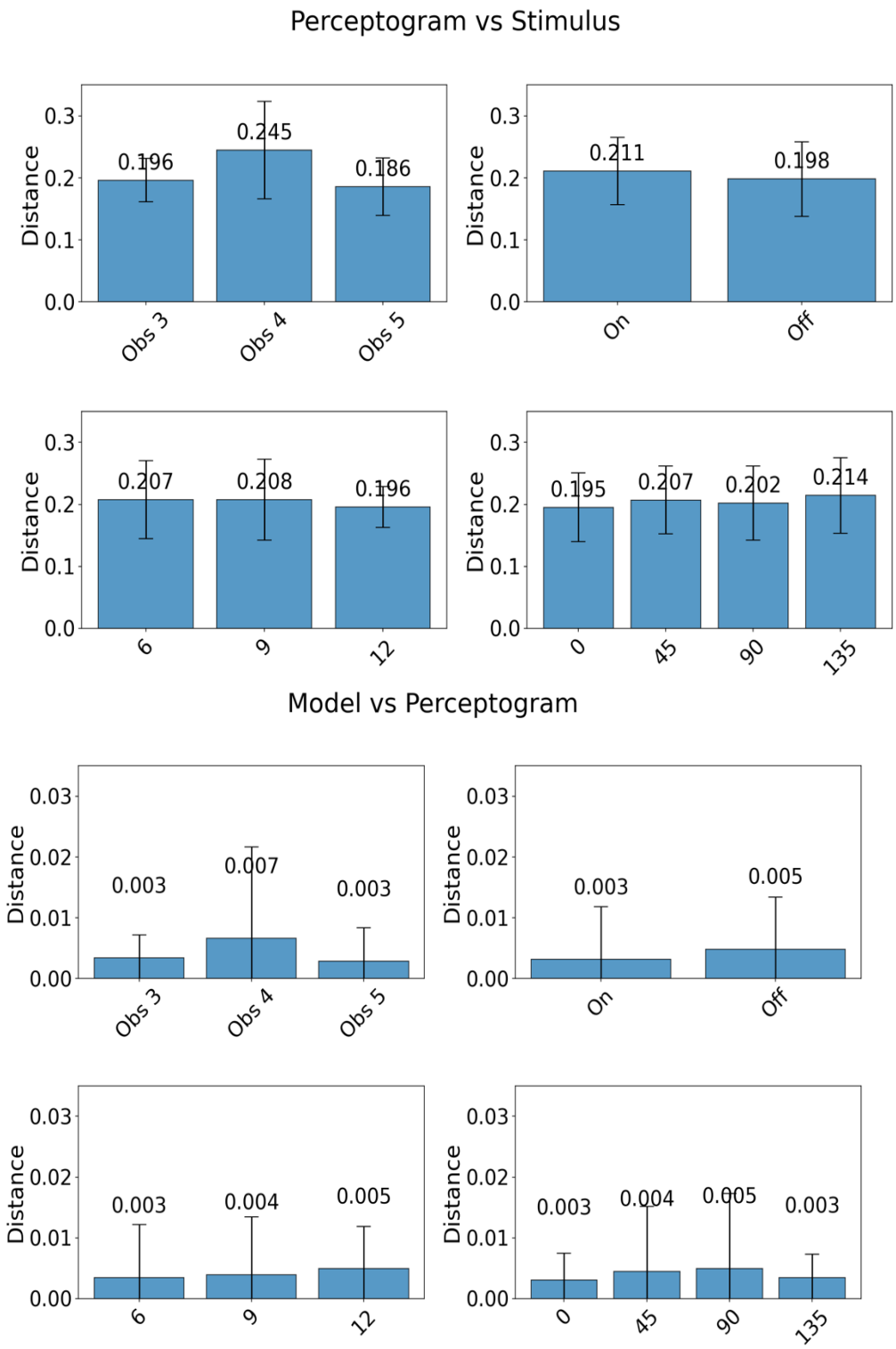


**Figure E4. Comparisons of the estimated perceptual distances between images:**
**Rows 1 & 2:** DISTS estimated perceptual distance between the measured perceptograms and stimulus gratings.
**Rows 3 & 4:** DISTS estimated perceptual distance between the model generated perceptograms and measured perceptograms.

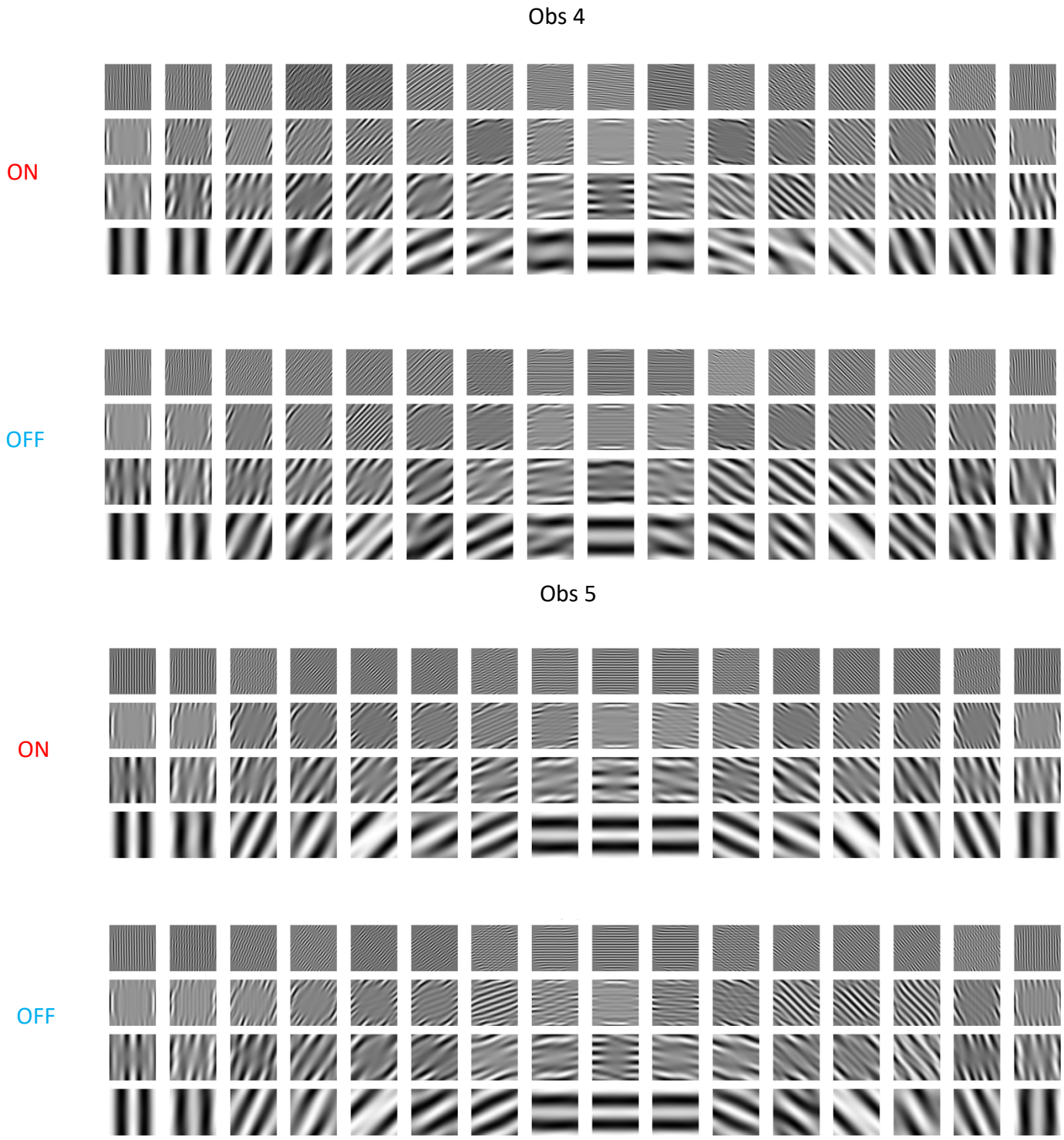


**Figure E5. Transformed AE filters for ON and OFF systems:**
Transformed filters for all spatial frequencies and orientations for Obs 4 and 5 who reported form distortions

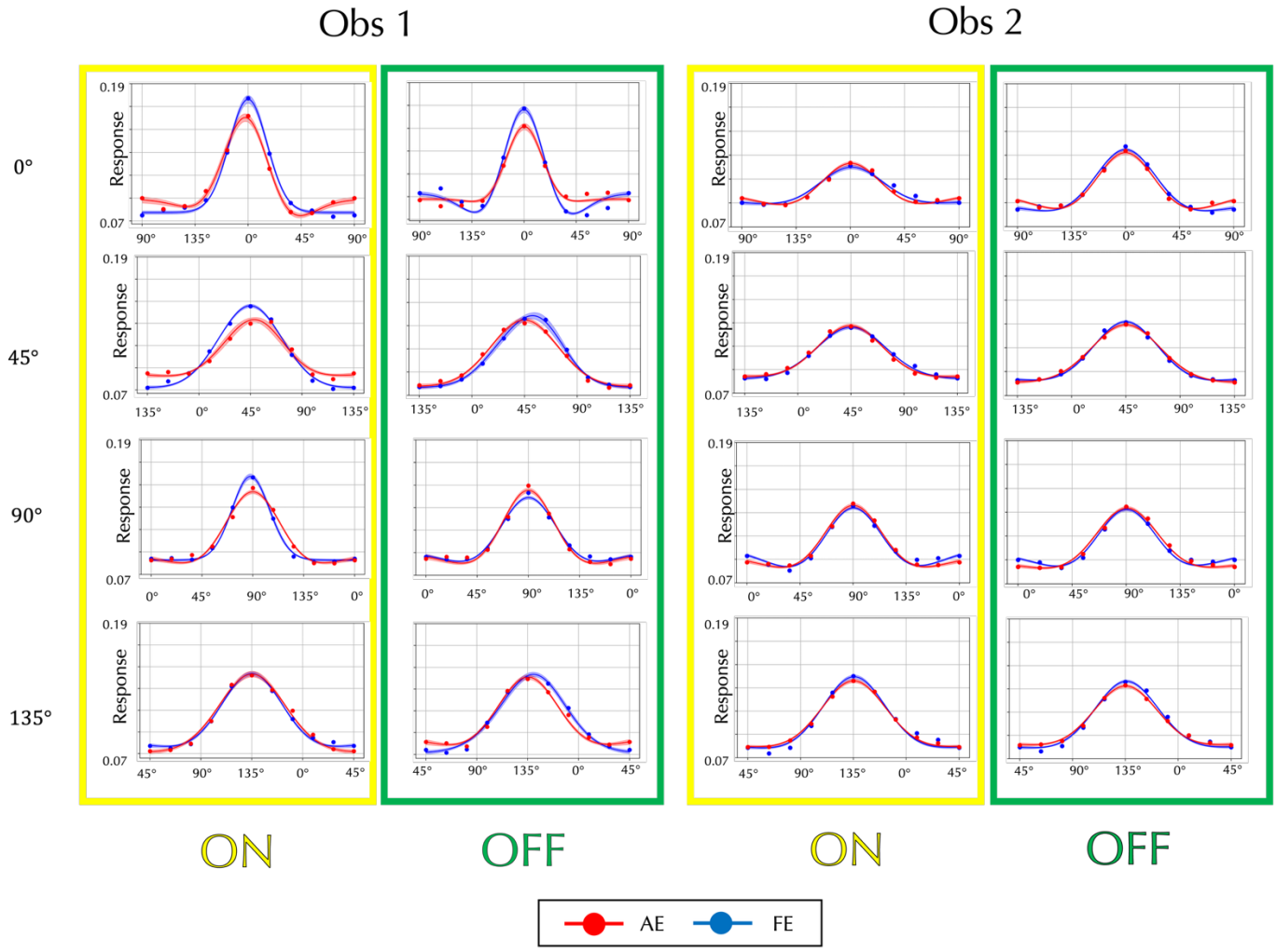


**Figure E6. Perceptual Orientation-tuning curves of individuals in the Non-distortion Group:** Results for amblyopic participants who did **not** report form distortions (Dashed boxes; Yellow: ON, Green: OFF). Each row corresponds to a different target orientation. Within each panel, response magnitude is plotted against physical orientation. Response magnitude is scaled to give unit area under the curve. Red and blue dots represent the mean responses (after 5,000 bootstrap resamples) for the amblyopic and fellow eye conditions, respectively. Solid traces are the best fitting von Mises functions, with shaded areas indicating ±1 standard deviation. Most of the mean R-squared values were 0.98 or higher.

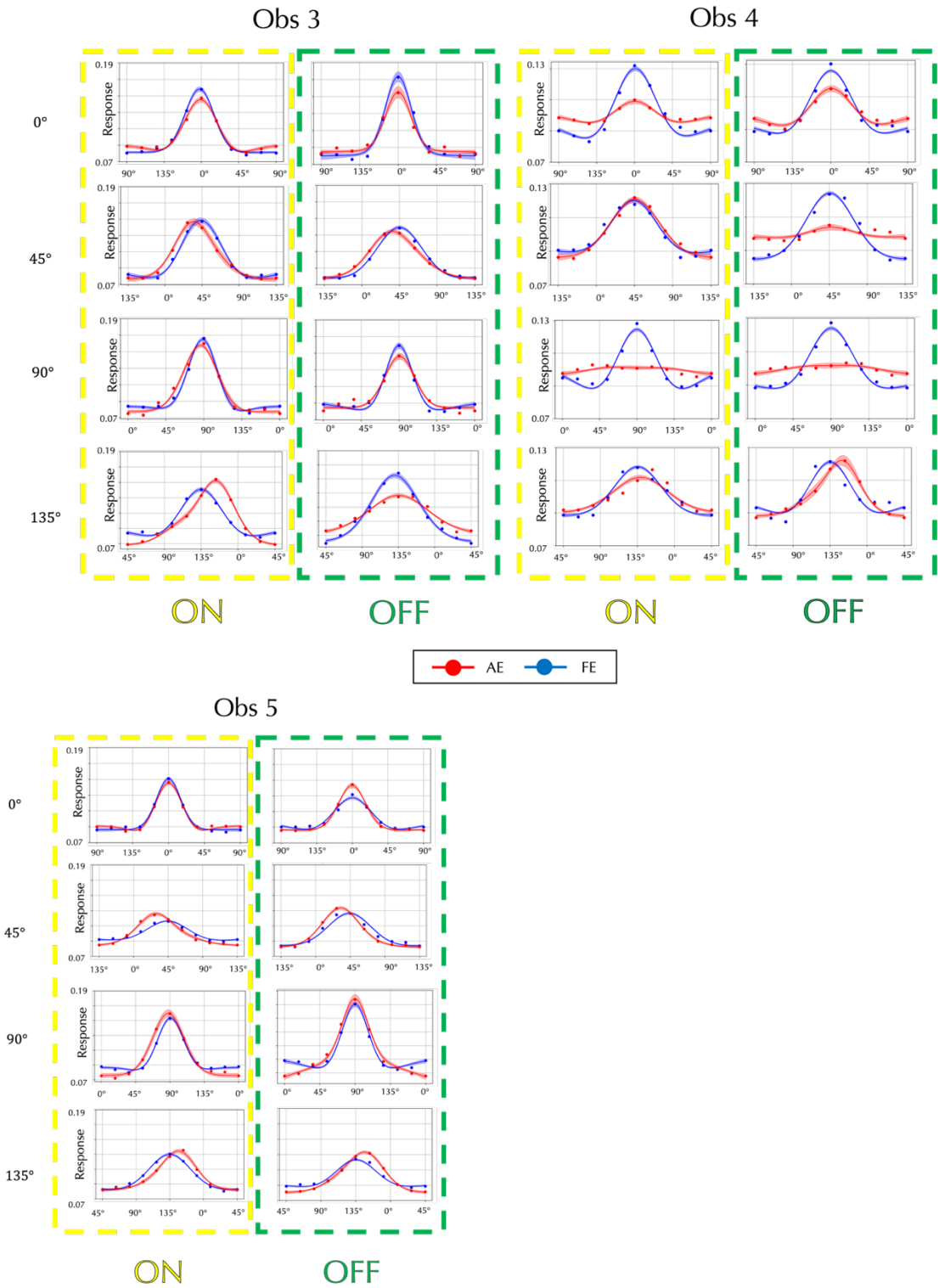


**Figure E7. Perceptual Orientation-tuning curves of individuals in the Distortion Group:** Results for amblyopic participants who **did** report form distortions (Dashed boxes; Yellow: ON, Green: OFF). Each row corresponds to a different target orientation. Within each panel, response magnitude is plotted against physical orientation. Response magnitude is scaled to give unit area under the curve. Red and blue dots represent the mean responses (after 5,000 bootstrap resamples) for the amblyopic and fellow eye conditions, respectively. Solid traces are the best fitting von Mises functions, with shaded areas indicating ±1 standard deviation. Most of the mean R-squared values were 0.98 or higher.

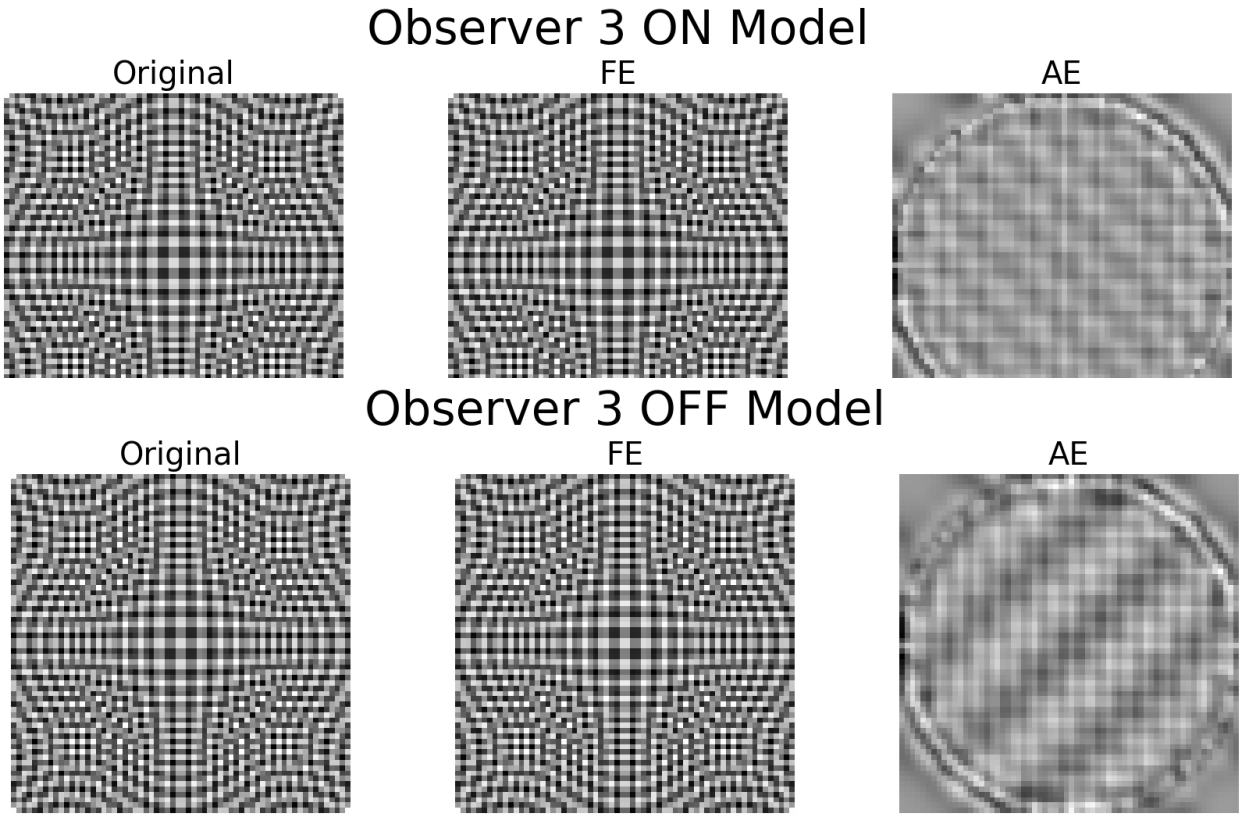


**Figure E8. 3D Shape-from-Texture stimuli with reconstructions generated by the FE and AE models.**